

Evaluation of Methodologies to Accelerate Corrosion Assisted Fatigue Experiments

N. Micone¹  · W. De Waele^{1,2}

Received: 30 July 2016 / Accepted: 26 October 2016 / Published online: 4 November 2016
© Society for Experimental Mechanics 2016

Abstract The corrosive nature of a marine environment is an important factor to be considered during the fatigue design of offshore structures. Thereto S-N curves must be determined in close to real conditions which is highly time consuming. It is hypothesized that if the corrosion process is accelerated at approximately the same rate as the fatigue frequency, testing time could be highly reduced. Corrosion acceleration is possible by modifying physical and/or electrochemical properties involved in the redox reactions. In this work the first option was chosen. Based on a literature review temperature and dissolved oxygen level were concluded to be the most influencing parameters. Several test scenarios with different combinations of sea water temperature and dissolved oxygen level have been defined. Corresponding S-N curves have been constructed for HSLA steel (type DNV F460) specimens immersed in natural seawater. The direct current potential drop technique was used to quantify damage evolution for all tested scenarios. Additionally, a reference S-N curve for immersed behaviour was determined at a temperature and frequency close to North Sea conditions. Comparison of the experimental results indicates that an average acceleration of the corrosion assisted fatigue damage process of around 80 % could be obtained.

Keywords Corrosion acceleration · Corrosion assisted fatigue · Testing · Potential drop · Temperature · Dissolved oxygen level

Introduction

The complex interaction of material, environment and loading conditions in offshore structures makes it challenging to run laboratory tests in real-life conditions (seawater at 7 °C average [1] and frequencies in the range of 0.1–2 Hz for the North Sea [2] e.g.). Notwithstanding physical and chemical characteristics of the seawater can be controlled, the corrosion assisted fatigue phenomenon is generally frequency dependent [3–5]. In offshore conditions, structures are subjected to very low frequencies which would lead to exorbitant testing time. Accelerating fatigue test frequencies in a laboratory environment is rather simple but it implies that the corrosion rate should also be accelerated. This approach is not always adopted, see e.g. [6]. In principle, an acceleration of the general corrosion process can be achieved by controlling electrochemical and/or physical parameters. This can be done during the mechanical fatigue test (coupled) or by pre-corroding a specimen followed by fatigue loading (uncoupled). An example of an uncoupled approach is pre-corrode specimens in the “salt spray” chamber. In such device, an acidified fog is sprayed on the specimen’s surface. This is done continuously or cyclically and additionally temperature can be increased to further enhance the acceleration effect [7]. These tests aim to analyze the corrosion resistance of (coated) metals exposed to a particular corrosive agent [8, 9]. However since the corrosion stage is done before fatigue testing, the interaction between environment and cyclic loading is missing which can lead to a very different fatigue resistance [6]. An attempt to couple this methodology to the fatigue test was reported in [10]. Clearly, a coupled methodology would be more representative and such approach will be further analyzed in this work.

✉ N. Micone
nahuel.micone@ugent.be

¹ Department of Electrical Energy, Systems and Automation, Ghent University, Technologiepark 904, 9052 Zwijnaarde, Belgium

² SIM vzw, Technologiepark 935, 9052 Zwijnaarde, Belgium

Some examples of accelerating the corrosion process by changing electrochemical parameters are reported in the following. An impressed direct electric current was used to accelerate the corrosion process in reinforced concrete bars [11] and to accelerate the corrosion assisted fatigue crack growth of an Fe440 steel [12] and an ASTM A333 grade 6 carbon steel [13]. In [14], the use of a galvanic couple (through a potentiostat controller) has allowed to predict the long-term corrosion of steel by an electrochemically accelerated aging technique. It was concluded that the weight loss of a specimen subjected to a 24 h accelerated corrosion test was equivalent to that evidenced after 90 days exposure to normal free corrosion conditions. In [15] the relation between the susceptibility of corrosion resistant steels to corrosion assisted fatigue and their electrochemical characteristics has been established. That study showed the possibility of controlling the corrosion rate through the modification of electrical parameters involved in the redox reactions. In [16] it was demonstrated that temperature and dissolved oxygen level increments allowed to accelerate the corrosion rate 20 times in terms of weight loss. These methodologies intend to increase the (uniform) corrosion rate. However when fatigue is added, the interaction between cyclic loads and the corrosion process might lead to a different result (faster or slower damage evolution). Notwithstanding all attempts to accelerate corrosion at the same rate as the fatigue load, a generic method for accelerated corrosion assisted fatigue has not yet been developed. [Acceleration of the corrosion process](#) section introduces the influence of different parameters involved in the corrosion process. Among others, temperature, pH and electrolyte composition are evaluated. The working principles of an environmental device and conditioning unit developed for accelerated corrosion assisted fatigue tests are discussed in [Device for controlled environment](#) section. Following, in [Experimental evaluation](#) section the experimental evaluation including the material properties, test procedure and environmental scenarios is explained. [Results and discussion](#) section presents the obtained S-N curves for all tested scenarios and the influence of temperature and dissolved oxygen level on damage evolution. Finally, conclusions are formulated in [Conclusions](#) section.

C	Material constant (–)
DA	Testing scenario where diffused air is injected to the electrolyte
DO	Dissolved oxygen level (mg/l)
f	Loading frequency (Hz)
HST ₄₅	High stress transition range - seawater at 45 °C (Mpa)
HST _{PD45}	High stress transition range - PD analysis seawater at 45°C (Mpa)
HST _{PD8}	High stress transition range - PD analysis seawater at 8 °C (Mpa)
k	Material constant (–)
LST ₄₅	Low stress transition range - seawater at 45°C (Mpa)

LST _{PD45}	Low stress transition range - PD analysis seawater at 45°C (Mpa)
LST _{PD8}	Low stress transition range - PD analysis seawater at 8°C (Mpa)
N	Number of cycles (–)
pH	Hydrogen potential (–)
R	Stress ratio (–)
ΔV_s	Stationary voltage increment (V)
σ_n	Fatigue limit obtained in air (MPa)
$\Delta\sigma$	Stress range (MPa)

Acceleration of the Corrosion Process

In order to enable acceleration of the corrosion phenomenon, knowledge of the most influencing parameters in this electrochemical process is needed. Gangloff [3] made an overview of modern laboratory methods for characterizing the corrosion assisted fatigue behaviour of metals in aqueous electrolytes. In his work, aspects related to testing methods (endurance and fracture mechanics approaches, e.g.) and schematics of different test setups were analyzed. Additionally the most important controlling parameters of the corrosion assisted fatigue phenomenon are discussed (see also [17–19]). Amongst them temperature, dissolved oxygen level, pH, electrolyte composition, electrochemical potential and frequency. Temperature and dissolved oxygen level, which are mutually dependent, have the highest influence on the corrosion rate [19].

In Fig. 1 it can be seen that increasing the temperature in open to the atmosphere systems, accelerates the corrosion process and reaches a maximum value at a certain temperature (80 °C in this example). After this ‘knee point’ the corrosion rate starts decreasing. The main reason is that at higher temperatures the dissolved oxygen (DO) level decreases which reduces the corrosion rate. The controlling parameter is no

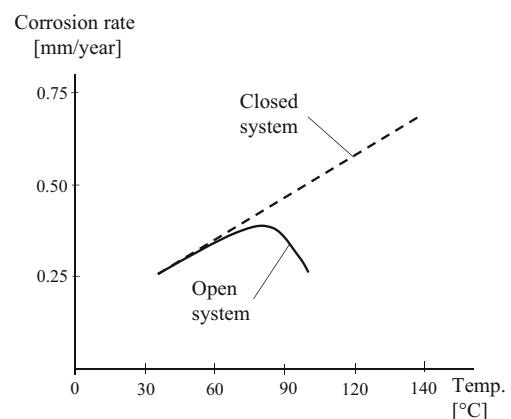


Fig. 1 Corrosion rate vs. temperature for iron in water containing dissolved oxygen (after [20])

longer the temperature but the dissolved oxygen level. In a closed environment, the oxygen cannot escape to the atmosphere and therefore the increase in corrosion rate is visible for a larger temperature range [17].

As long as the pH level is not highly reduced, this parameter is expected not to play an important role in the acceleration of the corrosion process. As shown in Fig. 2 very low pH values (acid) would be needed for this purpose (natural seawater has a pH of approximately 8). During fatigue testing, a too low pH might even prevent cracks initiate and encourage crack blunting [21, 22]. Controlling the pH level might be cumbersome since very small amounts of added acid might result in a very high decrease of the pH level and it is unclear whether this will accelerate corrosion assisted fatigue or rather retard crack initiation. The pH level has therefore not been selected as controlling parameter in this work.

Another factor that influences the corrosion damage evolution is the electrolyte composition. In [24] the corrosion behavior of a low carbon steel in different solutions (natural and synthetic seawater) has been analyzed concluding that the corrosion rate in a simple artificial 3.5% weight/volume (*w/v*) NaCl solution was higher (around 4 times, see Table 1) than in natural seawater. However, more complex synthetic solutions, as described in the ASTM D1141 standard [25] and recommended by the Marine Biological Laboratory (MBL) [26] e.g., showed a corrosion rate similar to natural seawater. Thus in order to obtain realistic results from a test, the solution chosen must also represent natural conditions, including chemical and physical properties. From this point of view natural seawater is a good alternative. However it has been indicated that calcareous deposits normally present in natural seawater can cause crack arrest [27] and its corrosiveness can change depending on the extraction point [14].

As mentioned higher, a potentiostat could be used to control the electrochemical potential and as a result the corrosion rate to a certain extent. This equipment is used to measure the potential evolution during corrosion assisted fatigue testing [28–30]. Special attention must be paid to the current flow and counter electrode size, since they are related to the size of the area on the specimen to be corroded. This approach is in this work not further considered.

Device for Controlled Environment

All factors discussed above define the aggressiveness of the environment and should be controlled and measured during testing in order to assure a close to real testing environment. Devices developed to run such tests were

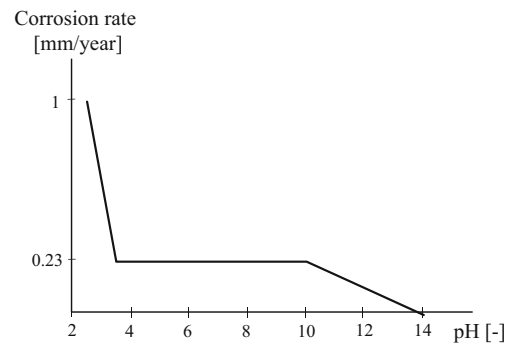


Fig. 2 Corrosion rate vs. pH level for iron exposed to aerated water at room temperature (after [23])

studied during the literature review stage. This revealed a wide range of possibilities. Some are based on simple working principles as putting the specimen in a rubber piece [31], permeating seawater in cotton attached to the specimen surface [4], or submerging the specimen into a corrosion cell [32–34]. Others are more complex systems capable of deaerating the testing solution [21], run tests in very hazardous situations [35, 36], high pressure hydrogen [37], or able to inject a NaCl fog onto the specimen's surface [38].

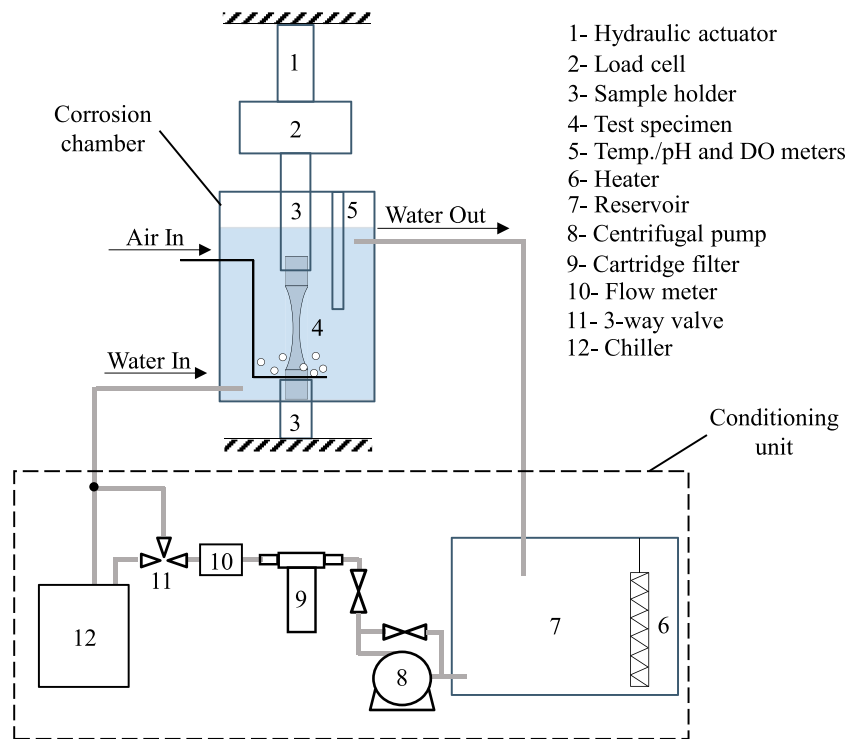
It was decided that the designed system should allow the user to simulate different conditions reflecting full submersion and splash zone tests as described in [6]. It should also allow to test different types of specimens according to e.g. ASTM 466 [39] for endurance fatigue tests, and ASTM 647 [40] for fracture mechanics fatigue tests. Additionally the setup should allow to control test parameters as flow rate, temperature, salinity and dissolved oxygen level of the seawater among others. The visibility of the specimen and the feasibility to apply multiple on/off-line instrumentation techniques to measure fatigue damage (potential drop, strain gauges, clip gauges e.g.) were also of high priority in the design stage. A detailed description of the design of the actual setup is given in [41].

In Fig. 3, the schematics of the installation are displayed. The seawater is stored in a PVC reservoir (7) during the test. For testing temperatures higher than room temperature, a heater (6) controlled by a PID controller is installed inside the reservoir. It allows to increase the temperature to a maximum of 45°C \pm 0.5°C. If testing

Table 1 Corrosion rates obtained for SAE 1006 steel in seawater [24]

Electrolyte	Natural seawater	ASTM D1141	MBL	3.5% NaCl
Corrosion rate (mm/year)	0.20	0.22	0.28	0.72

Fig. 3 Schematic of the corrosion-fatigue experimental setup



temperatures lower than room temperature have to be achieved, a chiller (12) can be used to cool the fluid down to $2^{\circ}\text{C} \pm 1^{\circ}\text{C}$. The water is then pumped (8) and filtered (9) using a cartridge filter of $100\ \mu\text{m}$. Between the filter and the chiller a flowmeter (10) is installed. Making use of a bypass (11), the testing flow rate is set at approximately $7\ \text{l/min}$. The seawater is pumped into the device at the bottom and flows out at the top. In this way a homogeneous temperature distribution is achieved. Inside the device an air diffuser is installed in order to saturate the water with air even at high testing temperatures.

As introduced before, it is essential to measure and control different chemical and physical parameters like temperature, pH, dissolved oxygen level and salinity. A microprocessor based pH controller ‘Hanna instruments pH 500’ with a measurement range from 0 to 14 pH (from -9.9°C to 120°C), a resolution of 0.01 pH (0.1°C) and an accuracy at 20°C of $\pm 0.02\ \text{pH}$ ($\pm 0.5^{\circ}\text{C}$) is used. A dissolved oxygen meter ‘Hanna Instruments HI 98193’ with a measurement range from 0 to $50\ \text{mg/l}$ dissolved oxygen, a resolution of $0.01\ \text{mg/l}$ and an accuracy of $\pm 1.5\%$ is also installed. The salinity is measured before, during and after each test making use of a seawater refractometer ‘Hanna instruments HI 96822’ with a measurement range of 0 to 150 ppt, a resolution of 1 ppt and an accuracy of $\pm 2\ \text{ppt}$. If salinity needs to be corrected, distilled water with or without the addition of sea salt can be used. For the correction of the pH level, hydrochloric

acid (HCl) and sodium hydroxide (NaOH) can be used. However a pH level of 8 ± 0.2 was measured in all analyzed scenarios and a correction was thus not needed. Typical (average) measured environmental parameters are shown in detail in [Experimental evaluation](#) section.

Photographs of the environmental device and conditioning unit illustrating the most important parts can be seen in Figs. 4 and 5(a) (b) respectively.

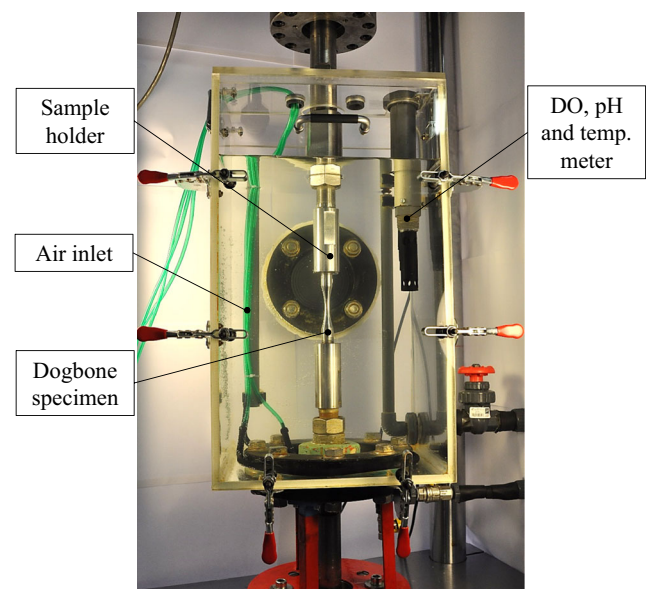


Fig. 4 Photograph of the environmental chamber

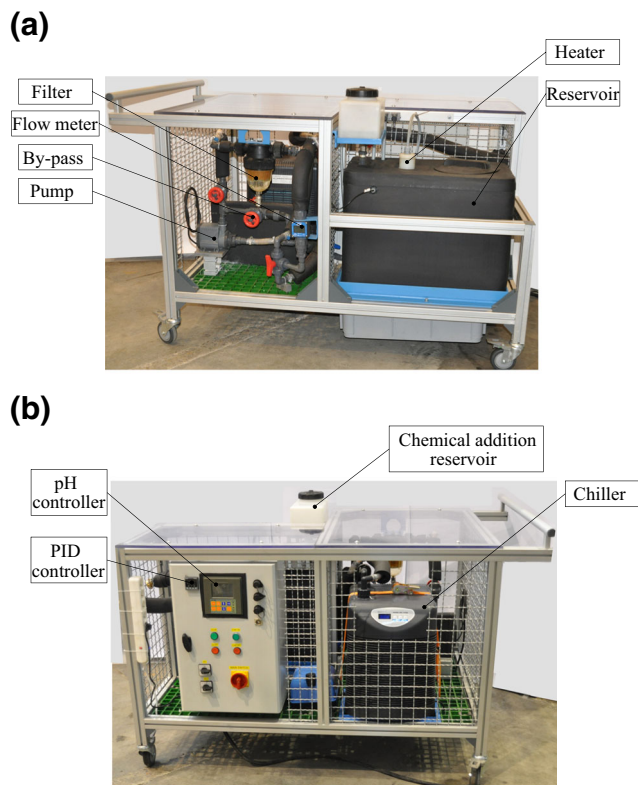


Fig. 5 a Conditioning unit back side b Conditioning unit front side

Used Seawater

As mentioned before, the composition of the electrolyte is very important. In this work, pre-filtered (5 μm) natural seawater from the North Sea coast of Belgium was used. Its chemical content is shown in Table 2.

In order to guarantee a constant condition of the seawater before each test, it was stored in 3 PVC containers of 1000 l each and continuously recirculated through a UV light (*MultiMax 11 W*) and a 5 μm cartridge filter. In this way physical and biochemical factors were kept constant.

Table 2 Chemical analysis of natural seawater used

Element	Concentration (mg/l)
Borium (B)	4.6
Calcium (Ca)	389
Potassium (K)	420
Magnesium (Mg)	1210
Sodium (Na)	10,700
Strontium (Sr)	7.2
Sulphate (SO ₄)	2500
Chlorides (Cl)	20,800
Bicarbonate (HCO)	170
Bromide (Br)	69

Experimental Evaluation

Material and Specimens

The material used in this work is an HSLA steel equivalent to grade NV F460, often used in offshore structures. Its microstructure, illustrated in Fig. 6, consists of ferrite and pearlite. The chemical composition (expressed in weight percentage) and the mechanical strength properties are presented in Tables 3 and 4 respectively.

Two dogbone shaped round bar fatigue specimen configurations were defined based on the ASTM E466 standard [39]. The first and standard configuration (Fig. 7(a)) is used to determine the S-N curves. The second configuration (Fig. 7(b)) is used for quantification of damage evolution by means of a direct current potential drop (DCPD) technique. In this configuration the length of the non-reduced section is longer to allow the electrical current flow more homogeneously through the specimen. The dimensions of both specimen configurations are shown in Figs. 7(a) and (b) respectively.

The specimens were extracted from seamless steel pipes with outer diameter 323.9 mm and wall thickness 25.4 mm. All of them were mirror polished with sandpaper in a sequence of 180, 220, 350, 800, 1200 and 2400 grits in order to reduce surface roughness and thus the stress concentration present. This delays fatigue crack initiation and reduces scatter in the results

Test Procedure

All tests were carried out using an MTS810 servo-hydraulic system equipped with a load cell of 100 kN capacity. Tests were performed in force-controlled mode. The stress ratio $R = 0.1$ and frequency $f = 10$ Hz were kept constant for all tests with the exception of the reference test for which a frequency of 0.2 Hz was chosen.

The standard specimens were subjected to constant amplitude fatigue with stress ranges from 340 to 500 MPa. Tests were conducted until failure in order to determine the

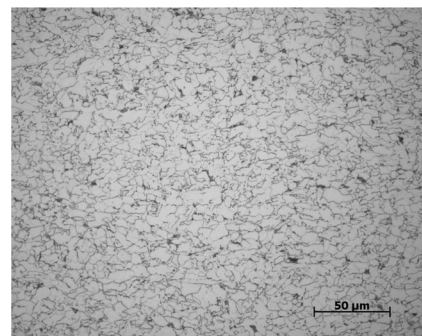


Fig. 6 Microstructure of the HSLA steel NV F460

Table 3 Chemical composition of NV F460 steel in wt.%

Material	C	Mn	Si	P	S	Cu	Ni	Cr	Mo
NV F460	0.08	1.24	0.24	0.01	0.001	0.05	0.21	0.05	0.005

S-N curves of the material. In parallel, the elongated specimens were used in a series of fatigue tests with stepwise increasing block loads, with the purpose of deriving a damage evolution curve for each of the analyzed situations. The stress ranges and number of cycles per block for these test series are summarized in Table 5. It has to be mentioned that before starting the fatigue test, the specimens were submerged in seawater at the corresponding environmental conditions until a fine uniform corrosion layer was visible. This lasted 1.5 h for the tests at 45°C and added diffused air (DA), 2 h for the tests at 45°C, 3 h for the tests at 15°C and 5 h for the tests at 8°C.

As mentioned before, different test conditions were realized by changing the temperature and dissolved oxygen levels. The testing scenarios are given in Table 6.

The pH level, temperature, salinity and dissolved oxygen level were measured and balanced (when required) as explained in the previous section.

Damage Evolution Monitoring

In order to monitor the damage evolution, the direct current potential drop concept was applied. As elaborated in detail in [42], the voltage evolution during a stepwise increasing block loading test (see Fig. 8(a)) is related to the cumulative fatigue damage (see Fig. 8(b)). In Fig. 8(b) two regions are separated by a dotted line which is drawn at the intersection of linear fitted curves (dash-dotted lines) to the lower and higher voltage regions. Stress values in the left region result in a limited voltage increment after a new loading block has started. This region is therefore defined as low dissipated energy region (LDE) and only a limited amount of fatigue damage is generated. For stress levels in the right region, a higher voltage increment is evidenced which is interpreted as significant damage generation. This region is therefore defined as high dissipated energy region (HDE).

For the application of the DCPD method, the direct current power source used was an autoranging Farnell AP60–150 with a maximum output power of 3 kW. The measurement instrument used was a nanovolt meter Agilent 34,420 with a

Table 4 Mechanical strength properties of NV F460 steel

Material	Yield stress, σ_y [MPa]	Ultimate tensile strength, σ_{UTS} [MPa]
NV F460	560	635

continuous integrating measurement method (Multi-slope III A-D Converter) and A-D Linearity of 0.00008% of reading +0.00005% of range.

Results and Discussion

Effects of Temperature and Oxygen on S-N Curves

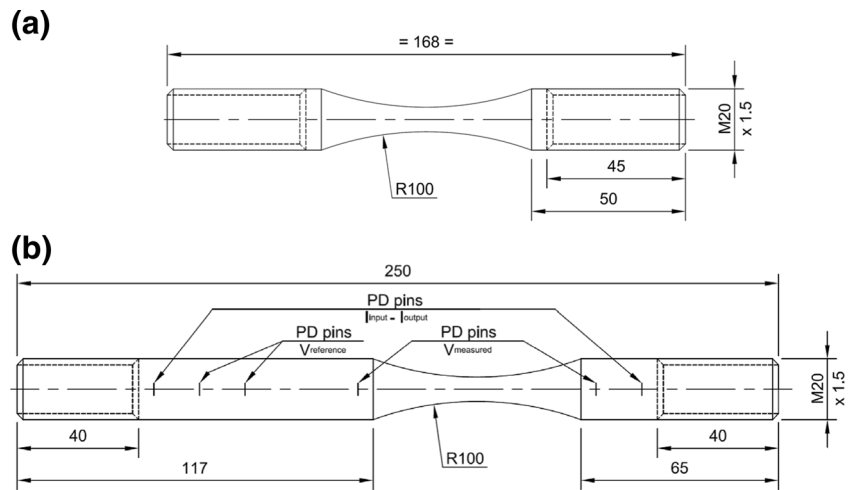
From the constant amplitude tests, the S-N curves of the material subjected to different environmental conditions were obtained according to the ASTM E 739–91 standard [43] and plotted together with the S-N curve obtained in air (see Fig. 9). The S-N curve obtained in air has a fatigue limit of approximately 440 MPa.

There is a significant influence of the environment on the fatigue resistance of the tested material which is generally explained by means of the anodic dissolution and hydrogen embrittlement effects [44]. The exposure time to the corrosive environment is longer at lower stress ranges resulting in a more pronounced influence on damage initiation whilst it is well known that most of the fatigue life of steel is spent in crack initiation. The evidenced life reduction at low stress ranges in a corrosive environment is furthermore in line with observations made during fatigue crack growth tests. It has been reported that closure mechanisms occurring at very low stress intensity factors and oxidizing environments provide a basis for enhanced corrosion debris formation by repeated breaking and compacting of the oxide as reported in [45] or by surface film rupture and preferential electrochemical attack at the ruptured sites [46].

For the tested stress ranges, and as generally expected, there is no clear fatigue limit in corrosion assisted fatigue tests [5, 47–50]. Among the evaluated situations, the most aggressive environment (i.e. with the shortest fatigue life) is obtained for seawater at 45°C with the addition of diffused air (DA). In comparison with the curve obtained at 15 °C, the endurance level was reduced with 40% at 470 MPa, with 30% at 400 MPa and with 20% at 340 MPa. Interestingly, the third evaluated situation (seawater at 45°C, orange curve) shows a transition from the S-N curve for seawater at 45°C with diffused air and the S-N curve for seawater at 15°C. It starts at a high stress range transition value (HST45) of 490 MPa approximately and finishes at a low stress range transition value (LST45) of 350 MPa approximately.

As reported before, the S-N curve for seawater at 45°C and diffused air represents the most damaging environmental condition. By comparing the S-N curves for seawater at 45°C and for seawater at 45°C with diffused air, it is possible to conclude that both temperature and oxygen play an important role in the damage process at higher stress ranges while the dissolved oxygen level is the main contributor at lower stress ranges (also see [20, 51]). A very limited influence of

Fig. 7 **a** Specimen dimensions in mm (standard version) **b** Specimen dimensions in mm (elongated version)



temperature on corrosion assisted fatigue crack growth rate at very low stress intensity values has been reported in [52].

Effect of Temperature and Oxygen on Damage Evolution

As reported in [42], the direct current potential drop technique can be used during stepwise block loading testing to evaluate the evolution of damage during a fatigue experiment. In this work the same technique was used for the comparison of fatigue damage evolution in all evaluated conditions. In Fig. 10, the voltage signals (which are a measure of the cumulated damage) recorded during the stepwise loading procedure detailed in [Experimental evaluation](#) section are plotted (after filtering them according to [42]). As expected, all studied environmental scenarios were more aggressive than conventional in air testing. The curve representative for the condition seawater at 45°C + diffused air shows an early damage activation and evolution compared to the condition seawater

at 15°C. Another interesting observation is that the same transition trends as shown in Fig. 9 can be seen. As a matter of fact, the transition points (HST_{PD45} and LST_{PD45}) of the testing condition seawater at 45°C lay very close to the ones reported in [Experimental evaluation](#) section. Additionally, at lower stress ranges all trend lines approach the one tested at 15°C.

Acceleration of Corrosion Assisted Fatigue with Respect to a Reference Condition

Notwithstanding the DCPD analysis presented so far allows to analyze the evolution of corrosion assisted fatigue damage in each evaluated scenario, it is not yet possible to link these results with the temperature and frequency expected in reality. As stated before, obtaining the S-N curve for this condition would lead to exorbitant testing time. A stepwise block loading test has been carried out at 8°C and 0.2 Hz according to the test procedure indicated in Table 4 with the aim of generating a reference damage evolution curve. The DCPD results can be seen in Fig. 11.

The so obtained curve has been compared to these obtained for specimens in seawater at 15°C and in air (both at 10 Hz). The reference curve shows a low stress range transition value (LST_{PD8}) of 320 MPa where the voltage increment is equal to that obtained for the specimen in seawater at 15°C and it tends towards the curve obtained in air at higher stress ranges showing a high stress range transition value (HST_{PD8}) of 500 MPa. These observations allow to construct the reference S-N curve as follows. The number of cycles to failure corresponding to the LST_{PD8} stress range is determined from the S-N curve for seawater at 15°C; the number of cycles to failure corresponding to the HST_{PD8} stress range is determined from the S-N curve for air at room temperature. Hypothesizing that these stress values and corresponding cycles to failure also belong to the reference

Table 5 Stepwise loading procedures

Stress range ($\Delta\sigma$) [MPa]	Block number	Block length @ 10 Hz [# cycles]	Block length @ 0.2 Hz [# cycles]
200	1	20,000	3000
330	2	15,000	2200
360	3	15,000	2200
390	4	15,000	2200
410	5	15,000	2200
430	6	15,000	2200
450	7	10,000	1500
460	8	10,000	1500
470	9	10,000	1500
480	10	7000	1000
490	11	7000	1000
500	12	7000	1000

Table 6 Testing scenarios and measured physical parameters

Scenario	Temperature [°C]	Diffused air [-]	Dissolved oxygen [mg/l]	pH [-]	Salinity [ppt]	Frequency [Hz]
S-N curves (10 Hz)						
1	15	No	6.2	8.03	35	10
2	45	No	3.7	7.98		
3	45	Yes	5.1	8.01		
Damage curves (10 Hz)						
4	15	No	6.2	8.03	35	10
5	45	No	3.7	7.98		
6	45	Yes	5.1	8.01		
Reference damage evolution curve (0.2 Hz)						
7	8	No	7.5	8.10	35	0.2

S-N curve it is possible to fit a curve of the following form (Basquin equation):

$$\Delta\sigma^k N = C$$

Where $\Delta\sigma$ is the stress range, N is the number of cycles until failure and k and C are constants. Making use of the generalized reduced gradient (GRG) solver algorithm, the constants were estimated as $k = 3.89$ and $C = 9.66E15$ (this parameter is normally expressed in its logarithmic form: $\log(C) = 15.98$).

Figure 12 shows the fitted reference S-N curve (blue dashed line) together with the curves obtained in air and in seawater at both 15°C and 45°C with diffused air. The datapoints used for the curve fitting procedure are shown as blue squares.

Assuming that the calculated reference curve is a good estimate for the S-N curve in real conditions (seawater 8°C and 0.2 Hz), it might imply that - in this work - environmental factors are more important than the frequency. This result was unexpected since in general one expects a certain frequency dependence in corrosion assisted fatigue tests; at least for crack growth based experiments [7]. Therefore an additional stepwise test at 8°C and 10 Hz has been carried out. Interestingly, the same damage evolution curve as the one

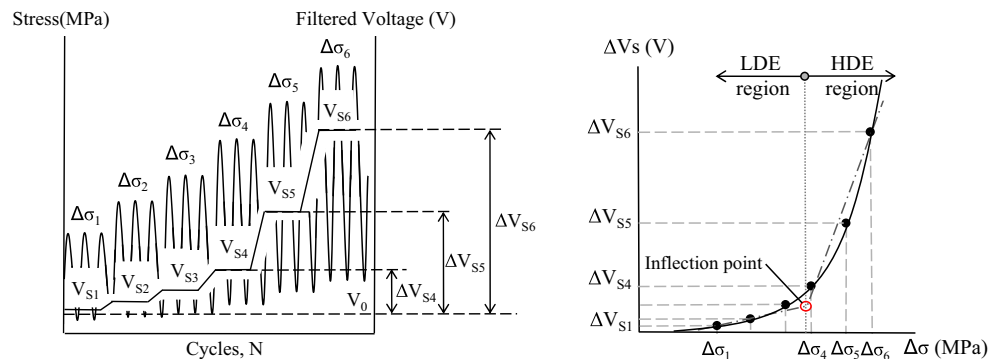
obtained at 8°C and 0.2 Hz was obtained. This strengthens the hypothesis that the frequency does not play a significant role for the evaluated conditions. A similar response was also reported in [3] for crack growth based tests. In any case, the S-N curve for such particular condition should be constructed by the traditional method in order to verify this hypothesis.

Comparing the reference S-N curve to the S-N curve obtained at 45°C with diffused air, a significant acceleration of the corrosion assisted fatigue damage process (on average 80%) was obtained. Again, such phenomenon is much more efficient at higher than at lower stress ranges.

Conclusions

In this work, the need of running accelerated corrosion assisted fatigue tests has been highlighted. To do so, the electrochemical reactions that take place between sample and environment must be speeded up together with the testing frequency. On the one hand, one can use a current flow between the specimen and a counter electrode to change the speed at which the reactions take place. On the other hand, chemical and/or physical parameters can be modified. A literature review revealed that temperature

Fig. 8 **a** Typical stepwise block loading scheme for damage evolution analysis **b** Voltage increase versus stress range from Fig. 8a



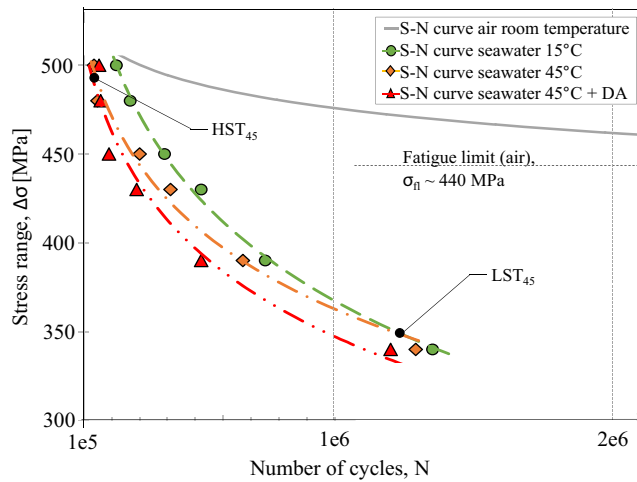


Fig. 9 S-N curves obtained under different environmental conditions

and dissolved oxygen level are of major relevance. Therefore these were used as the variable environmental parameters in this investigation.

An environmental device allowing to perform fatigue tests in controlled environmental conditions has been designed and build. This setup was used to run a series of tests at different environmental conditions. Analyzing the determined S-N curves indicated that all analyzed scenarios show an important influence of the environment on the corrosion assisted fatigue process. No fatigue limit was found in the tested stress range band. It was concluded that both temperature and dissolved oxygen level play an important role in the acceleration of the damage process at higher stress ranges, while the addition of diffused air is the most important parameter at lower stress ranges.

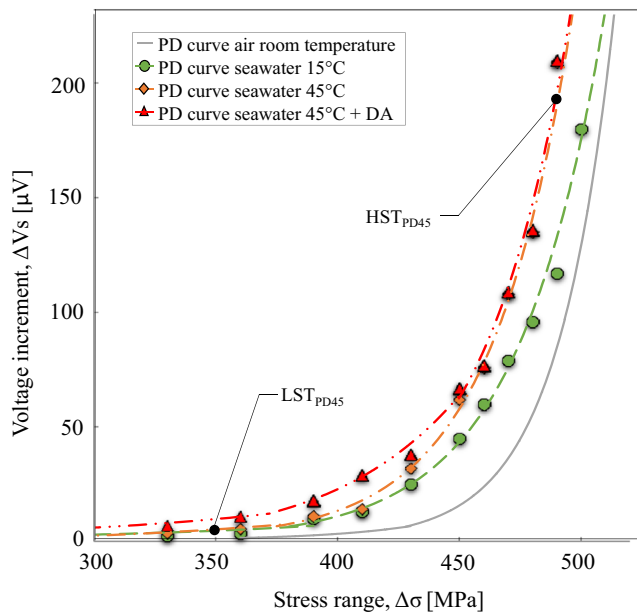


Fig. 10 ΔV_s - $\Delta\sigma$ curves obtained at different environmental conditions ($f = 10$ Hz)

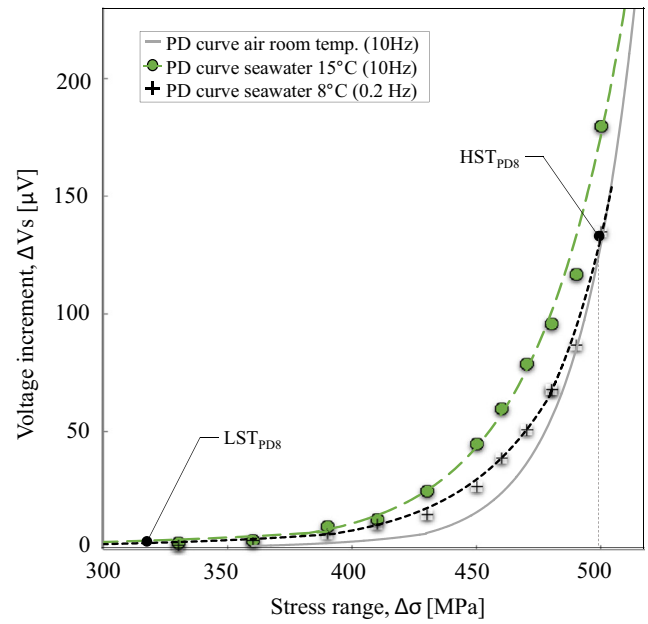


Fig. 11 ΔV_s - $\Delta\sigma$ curves obtained at real ($f = 0.2$ Hz) and testing conditions ($f = 10$ Hz)

The direct current potential drop concept was applied to a series of dedicated tests in order to obtain a damage evolution curve for each of the evaluated environmental conditions. From this analysis, the same high and low stress transition ranges as the ones highlighted in the analysis of the S-N curves were identified. This corroborates the feasibility of this technique for the evaluation of corrosion assisted fatigue. Additionally, the construction of an S-N curve obtained from the DCPD analysis of a test in close to real conditions was discussed. The obtained curve suggests certain frequency independence.

By comparing the most and least severe environmental conditions, the tested methodology was able to accelerate

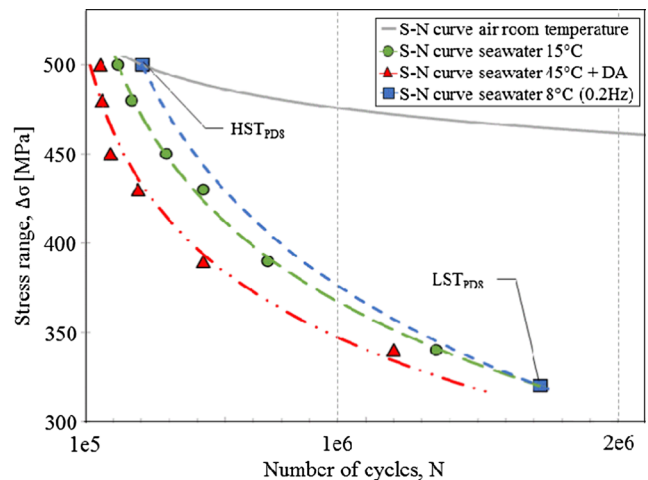


Fig. 12 S-N curves obtained according the traditional approach for seawater at 15°C-10 Hz and 45°C + DA-10 Hz and calculated from the DCPD analysis for seawater at 8°C-0.2 Hz

the corrosion assisted fatigue damage significantly (up to 80% on average).

Additional work is needed to confirm the previous observations, and in particular to evaluate whether or not corrosion assisted fatigue of unnotched offshore steels is frequency dependent. In addition, work is ongoing to apply the methodology developed in this work to notched specimens.

Acknowledgments The authors would like to acknowledge the financial support of VLAIO (Agency for innovation and business - grant n°131797) and SIM (Strategic Initiative Materials in Flanders – MaDurOS program).

References

- Dover W.D, Dharmavasan S, Brennan F.P, Marsh K.J (1995) Fatigue crack growth in offshore structures. ISBN 0947817786. EMAS, UK.
- Thorntonbank golfddata 2003–2013 (2016) Meetnet vlaamse banken.
- R.P G (2005) Environmental cracking-corrosion fatigue. In: Baboian R (ed) Corrosion tests and standards: application and interpretation, 2nd edn. ASTM, USA, pp. 302–321
- Prakash R.V, Dhinakaran S (2013) Estimation of corrosion fatigue-crack growth through frequency shedding method. ASTM International Journal Vol. 9, No. 5.
- Procter R.P.M (1991) Atlas of stress-corrosion and corrosion fatigue curves. Br Corr J Vol. 26 No. 1. ISBN0871703742.
- Palin-Luc T, Perez-Mora R, Bathias C, Dominguez G, Paris P, Arana J (2010) Fatigue crack initiation and growth on a steel in the very high cycle regime with sea water corrosion. Eng Fract Mech 77:1953–1962
- C.L M (2005) Cabinet tests. In: Baboian R (ed) Corrosion tests and standards: application and interpretation, 2nd edn. ASTM, USA, pp. 302–321
- ASTM B117 (2003) Standard practice for operating salt spray (fog) apparatus. ASTM.
- ASTM G85 (2009) Standard practice for modified salt spray (fog) testing. ASTM.
- LeBozec N, Thierry D (2015) A new device for simultaneous corrosion fatigue testing of joined materials in accelerated corrosion tests Materials and Corrosion:66 No. 9
- Fujian T, Zhibin L, Genda C, Weijian Y (2014) Three-dimensional corrosion pit measurement and statistical mechanical degradation analysis of deformed steel bars subjected to accelerated corrosion. Constr Build Mater 70:104–117
- Kelita S, Raghava G, Vishnuvardhan S, Ramesh Babu C (2015) Accelerated Corrosion Fatigue Crack Growth Studies on IS 2062 Gr. E 300 Steel. International Journal of Science and Engineering Applications Volume 4 Issue 3, ISSN-2319-7560 (Online).
- Aarathi P.S, Raghava G, Vishnuvardhan S, Surendar M (2015) Accelerated Corrosion Fatigue Studies on SA 333 Gr.6 Carbon Steel. IJRSET journal Vol. 4, Special Issue 6.
- Jung-Gu K, Yong-Jae Y, Jeong-Kun Y (2005) Prediction of long-term corrosion and mechanical behaviors of steel in seawater by an electrochemically accelerated aging technique. Met Mater Int 11(3): 209–214
- Khoma M. S, Pokhmurs'kyi V. I (2003) Changes in the electrochemical characteristics of corrosion-resistant steels at the beginning of the process of corrosion-fatigue damage. Mater Sci 39(1):9–14.
- Yousuke Y, Junya T, Mikihiro H, Itoh Y (2013) Corrosion Deterioration Characteristics of Structural Steel by accelerated exposure test system under the water. NACE international East Asia & Pacific Rim Area Conference & Expo 2013 (Kyoto Japan) 19:21.
- Stephen D. Cramer, Bernard S. Covino, Jr. (2003) ASM Handbook Volume 13A - Corrosion Fundamentals, Testing, And Protection. ISBN: 9780871707055, ASM international.
- Shreir L. L, Jarman R.A, Burstein G.T (2000) Corrosion Vol 1 3rd edition. ISBN: 978-0-08-052351-4, BH Oxford.
- Hagn L (1988) Life prediction methods for aqueous environments. Mater Sci Eng A 103:193–205
- Revie R. W, H.H U (2008) Corrosion and corrosion control. An introduction to corrosion science and engineering, 4th edn. Wiley-interscience, New Jersey
- Pargeter R, Baxter D, Holmes B (2008) Corrosion fatigue of steel catenary risers in sweet production. OMAE:2008–57075
- Woollin P, Pargeter R, Maddox S (2004) Corrosion fatigue performance of welded risers for deepwater applications. Corrosion 2004–04144.
- DOE fundamentals handbook (1999) Doe-HDBK-1015/1-93. Chemistry Vol 1:2
- Möller H, E.T B, Froneman H (2006) The corrosion behavior of low carbon steel in natural and synthetic seawaters. The Journal of the South African institute of Mining and Metallurgy 106:585–592
- ASTM D1141–98 (2013) Standard practice for the preparation of Substitute Ocean water. ASTM.
- G.M C (1975) Formulae and methods VI. Woods Hole, MA, The Marine Biological Laboratory
- Knop M, Heath J, Sterjovski Z, S.P L (2010) Effects of cycle frequency on corrosion-fatigue crack growth in cathodically protected high-strength steels. Procedia Engineering 2:1243–1252
- Imanian A, Modarres M (2015) A thermodynamic entropy approach to reliability assessment with applications to corrosion fatigue. Entropy 17(10):6995–7020
- Zuo-Yan Y, Dao-Xin L, Xiao-Hua Z, Xiao-Ming Z, Ming-Xia L, Zhi Y (2015) Corrosion fatigue behavior of 7A85 aluminum alloy thick plate in NaCl solution. Acta Metallurgica Sinica (English Letters) 28(8):1047–1054
- Campbell L, Yuanfeng L (2000) Methods and devices for electrochemically determining metal fatigue status. Patent US006026691A.
- Shu-Xin Li, Akid R (2013) Corrosion fatigue life prediction of a steel shaft material in seawater. Eng. F Analysis S1350–630700280-X.
- Mohamed A, J.R C, W.F C (2013) Corrosion fatigue of alloys containing chromium and molybdenum. Int J Eng Sci (IJES) 2(6): 111–121
- Michailidis N, Stergioudi F, Maliaris G, Tsouknidas A (2014) Influence of galvanization on the corrosion fatigue performance of high-strength steel. Surf Coat Technol 259:456–464
- Toledano Prados M, Galan Diaz J.J, Conde Del Campo A, Arenas Varas M. A (2012) Device for corrosion and fatigue testing. Patent WO2012/146819 A1.
- McMaster F, Thompson H, Zhang M, Walters D, Bowman J (2007) Sour service corrosion fatigue testing of flowline welds. OMAE: 2007–29060
- Wang J, Li X (2014) A Phenomenological Model for Fatigue Crack Growth Rate of X70 Pipeline Steel in H₂S Corrosive Environment. J. Pressure Vessel Technol 136(4), 041703.
- Bruchhausen M, Fischer B, Ruiz A, González S, Hähner P, Soller S (2014) Impact of hydrogen on the high cycle fatigue behaviour of Inconel 718 in asymmetric push-pull mode at room temperature. Int J Fatigue 70:137–145
- Leidinger D, Holper B, Sommitsch C (2015) Construction of a corrosion test device for the installation in a rotating bending

- machine for corrosion fatigue tests of Cr-Mn-N austenitic steels used in the oil-field industry. *BHM* 160(9):419–425
39. ASTM E 466–96 (2002) Standard practice for conducting force controlled constant amplitude axial fatigue tests of metallic materials. ASTM.
 40. ASTM 647 (2014) Standard test method for measurement of fatigue crack growth rates. ASTM.
 41. Delmotte E., Micone N, De Waele W (2015) Testing methodologies for corrosion fatigue. *Sustain. Constr. Des. J.*, vol.6, No. 3.
 42. Micone N, De Waele W (2016) On the application of Infrared Thermography and Potential Drop for the accelerated determination of an S-N curve. *Experimental mechanics*. Manuscript number EXME-D-16-00149 (accepted for publication).
 43. ASTM E 739–91 (2004) Standard practice for statistical analysis of linear or linearized stress-life (S-N) and strain-life (e-N) fatigue data. ASTM.
 44. Dong-Hwan K, Jong-Kwan L, Tae-Won K (2011) Corrosion fatigue crack propagation of high-strength steel HSB800 in a seawater environment. *Procedia Engineering* 10:1170–1175
 45. Suresh S, G.F Z, R.O R (1981) Oxide-induced crack closure: an explanation for near-threshold corrosion fatigue crack growth behavior. ASME and the metallurgical society of AIME Volume 12A:1435
 46. Haiyun H (1997) Fatigue and corrosion fatigue crack growth resistance of RQT501 steel. A Dissertation Submitted to the University of Sheffield for the Degree of Doctor of Philosophy in the Faculty of Engineering
 47. Hudak S, Robledo G, Hawk J (2011) Corrosion-fatigue performance of high-strength riser steels in seawater and sour brine environments. *OMAE*:2011–50171
 48. DNV-RP-C203 (2014) Fatigue design of offshore steel structures. DNV.
 49. BS 7191 (2005) British standard specification for weldable structural steels for fixed offshore structures. BS.
 50. Shipilov S.A (2005) Corrosion fatigue. *WIT Transactions on State of the Art in Science and Engineering*, Vol 1, WIT Press ISSN 1755–8336 (on-line).
 51. Schijve J (2009) *Fatigue of Structures and Materials*, 2nd edition. ISBN 9781402068072.
 52. Romaniv O.N, Vol'demarov A.V, Nikiforchin G.N (1981) Factors in acceleration of crack growth during corrosion fatigue of high-strength steels. *Mater Sci* 16: 406. doi:10.1007/BF00724469.